Received: 8 November 2023 | Accepted: 16 May 2025

DOI: 10.1002/hem3.70170

ARTICLE

HemaSphere eha

A spheroid model that recapitulates the protective role of the lymph node microenvironment and serves as a platform for drug testing in chronic lymphocytic leukemia

Elisa Lenti[1,^] | Edoardo Visentin[1,^] | Engin Bojnik[2,^] | Alessia Neroni[1] | Martina Franchino[1] | Daniela Talarico[1] | Nicolò Sacchetti[1] | Lydia Scarfò[2,3] | Aurora Maurizio[4] | Jose Manuel Garcia-Manteiga[4] | Paolo Ghia[2,3] | Andrea Brendolan[1]

Correspondence: Paolo Ghia (ghia.paolo@hsr.it) and Andrea Brendolan (brendolan.andrea@hsr.it)

Abstract

Chronic lymphocytic leukemia (CLL) B cells are characterized by a propensity to undergo rapid apoptosis when cultured in vitro, underscoring the importance of the tissue microenvironment for disease survival. One of the major limitations in studying the role of the microenvironment in tumor development and drug response is the inadequacy of conventional two-dimensional (2D) in vitro assays to physiologically reconstruct the complex spatial organization and interactions of cells in their natural lymphoid niches. To overcome this limitation, we developed a novel in vitro 3D lymph node-like spheroid model of the leukemic microenvironment by culturing human CLL cells with fibroblastic reticular cells (FRCs). FRCs are a key structural component of secondary lymphoid organs and are emerging as crucial players in tissue homeostasis and immune responses. Our results demonstrate that CLL spheroids maintain the physiological cellular ratio between FRCs and leukemic cells over time and protect tumor cells from apoptosis by mimicking the protective effects of the microenvironment. This was further demonstrated by venetoclax treatment that showed reduced apoptosis in 3D compared to a 2D setting. Importantly, the spheroids promote a gene expression profile more aligned with that of CLL cells in lymphoid tissues. The spheroid model provides a straightforward, quick-to-use platform for investigating drug efficacy under conditions that better replicate the natural lymph node microenvironment. This 3D lymph node-like spheroid model could serve as a valuable tool for studying tumor biology and the protective effects of the stromal microenvironment, and for testing therapeutic strategies in a more clinically relevant setting.

INTRODUCTION

Chronic lymphocytic leukemia (CLL) is characterized by the accumulation of monoclonal, mature $CD5^+$ B cells in the peripheral blood (PB) and in protective microenvironmental niches, such as the bone marrow (BM) and secondary lymphoid organs (SLOs).[1] In recent years, treatments for patients with CLL have progressively shifted toward novel drugs targeting the B-cell receptor signaling pathway such as inhibitors of Brüton's tyrosine kinase (e.g., ibrutinib) or antiapoptotic proteins such as BCL2 (e.g., venetoclax) in addition to chemotherapy.[2] Despite their impressive efficacy in controlling the disease, in particular in the case of BCL2 inhibitors, they appear to be less effective to eradicate malignant CLL cells in the context of lymphoid tissues in particular in lymph nodes (LNs).[3] In these protective niches, interactions with cells of the microenvironment promote tumor cell survival, drug-resistance, and disease progression.[4–10] To date, researchers have relied on animal models and two-dimensional (2D) culture systems to test drug efficacy. However, in vivo approaches are time-consuming, costly, ethically controversial, and often do not fully recapitulate all features of human disease. In addition, 2D culture systems represent an oversimplification of the LN microenvironment and do not recapitulate the 3D architecture of the native tissue, its

[1]Lymphoid Stromal Cell Biology Unit, Division of Experimental Oncology, IRCCS San Raffaele Scientific Institute, Milan, Italy
[2]B-Cell Neoplasia Unit, Division of Experimental Oncology, IRCCS San Raffaele Scientific Institute, Milan, Italy
[3]Università Vita-Salute San Raffaele, Milan, Italy
[4]Center for Omics Sciences, IRCCS San Raffaele Scientific Institute, Milan, Italy
^These authors contributed equally to this study.

protective effects, and the complexity of cellular interactions, leading to an overestimation of the sensitivity and toxicity of therapeutics. The LN microenvironment is composed of numerous cell types, including nonhematopoietic stromal cells also known as fibroblastic reticular cells (FRCs), which represent 5% of the total cells, provide survival and proliferation signals (e.g., BAFF) and chemokines (e.g., CXCL13) for hematopoietic cells and produce the extracellular matrix (ECM), a structural support that acts as a reservoir for signaling molecules and growth factors.[11–18] The supportive role of the microenvironment and the growing knowledge of the pathophysiology of CLL have reinforced the importance of developing appropriate 3D culture models that mimic the tumor microenvironment and may improve the in vitro evaluation of drug responses, overcoming some of the limitations of traditional 2D models. A number of 3D culture models have been developed, including tumor organoids and the use of scaffolds cultured in bioreactors to recapitulate physiological flow.[19–22] Despite their promising capabilities, these 3D models require specialized materials and technologies, are time-consuming, and are not suitable for high-throughput screening (HTS). Spheroids are an alternative approach developed for evaluating drug efficacy in solid tumors, as they favor interactions with the microenvironment while providing the ability to perform HTS.[23–25] However, an easy-to-use HTS physiological in vitro system for accurately predicting the efficacy of standard and novel therapeutic regimens for CLL is still under development. Recently, CLL T cell interactions were studied in a spheroid model that mimics some of the features of the LN.[26]

Here, we present a reliable 3D multicellular spheroid system suitable for evaluating the protective effects of the stromal microenvironment and assessing drug efficacy in conditions more similar to those of the native CLL microenvironment. Specifically, we developed an LN-like spheroid model by culturing human CLL B cells and lymphoid FRCs to recapitulate some cellular and structural features of the LN microenvironment. We demonstrate that spheroids are permeable to small molecules, maintain the physiological cell ratio of stromal and leukemic cells, protect tumor cells from apoptosis by mimicking the protective effects of the microenvironment, and induce CLL cells to express molecular signatures reminiscent of CLL cells isolated from the LN, ultimately mimicking the protective effect of a physiological microenvironment.

RESULTS

Replicating the lymphoid tumor microenvironments using spheroids

To develop a 3D model recapitulating a leukemic lymphoid microenvironment suitable for drug efficacy testing, we generated spheroids containing leukemic and lymphoid FRCs. For the preparation of spheroids, collagen type I was used as a biomimetic matrix because it is an ECM protein found in all SLOs, is an excellent substrate for cell adhesion due to its integrin-binding sites, and is widely used for tissue engineering applications.[27–29] To prepare spheroids, human primary CLL cells were suspended in a collagen type I solution and plated as hanging drops either alone or together with FRCs of mouse or human origin (Figure 1A). We decided to develop in parallel spheroids with either murine or human FRCs, as the former are largely available in many laboratories, while human FRCs are more limited, but more physiological.

Murine FRCs were isolated from the spleen of reporter mice expressing YFP and were visualized using anti-YFP antibodies, whereas human FRCs were established from human LN and were revealed by staining for the glycoprotein Podoplanin (PDPN/GP38). As the percentage of FRCs in LNs has been estimated to be around 5% of the total cellular content, we performed our experiments using a 1:20 ratio of FRCs to CLL cells (FRC:CLL) to provide a more physiological representation of the in vivo situation.[17] After 24 h, the resulting collagen-based structures generated using only CLL cells showed a spherical shape with sharp edges, minimal contraction, and stable dimensions throughout the experimental period (Figure 1B,C). On the other hand, spheroids generated with CLL and FRCs showed a significant decrease in volume caused by the contraction of collagen fibers by FRCs and stabilized at a diameter of approximately 300–400 µm (Figure 1B,C).

Immunofluorescence analysis was performed at 24, 48, and 96 h following spheroid formation. CLL cells were visualized by staining with anti-CD45 antibodies, whereas murine and human FRCs were identified using anti-YFP and PDPN antibodies, respectively (Figure 1D,E).

After 48 h, spheroids containing murine FRCs exhibited three distinct regions: the outer ring, an intermediate zone, and the core. FRCs in these regions displayed varying appearances and arrangements, likely reflecting the heterogeneity of the FRC population used. In the outer ring, murine FRCs appear flattened and elongated, forming a capsule-like ring (Figure 1D; arrows). In the intermediate zone, FRCs were oriented toward the center and loosely distributed compared to those in the outer ring, whereas in the core, they were more densely packed (Figure 1D). In contrast, spheroids with human FRCs did not form a capsule-like ring, and the distribution of the cells was more homogeneous throughout the spheroid. Importantly, GP38/PDPN signal increased over time revealing the presence of FRCs interspersed within CLL cells by 96 h (Figure 1E).

We then tested whether spheroids are suitable for assessing drug efficacy in a more physiological setting. To this end, we first performed a permeabilization assay using CMTPX CytoTrace™, a red fluorescent dye that can permeate cells and has a similar molecular weight to many drugs currently used in the clinical setting such as ibrutinib and venetoclax. After spheroid formation, CMTPX was added to the culture for 12 h. Confocal analysis showed a brighter signal on the outer region of both murine and human spheroids, though the signal when using mouse FRCs was stronger, with dye-positive cells also present in the inner part (Figure 1F). Altogether, these findings indicate that spheroids are permeable to small molecules, making them a model for drug testing.

Spheroids retain physiological cellular ratio and support long-term leukemia survival

Unlike CLL cells, which do not proliferate in vitro and tend to die rapidly in the absence of stimuli, FRCs expand in standard 2D cultures. Cell proliferation can affect cell ratios and compromise assay predictability and reproducibility, as well as cell viability, as proliferating cells consume media and excrete waste. To determine if and how cell ratio changes in 3D cultures compared to 2D cultures, we counted the number of cells in spheroids prepared with and without murine FRCs only, 24 and 96 h after spheroid formation. We found that the total number of cells in the spheroids decreased in the presence of FRCs, likely due to fibroblast contraction that reduced spheroid size (Figure 2A). However, at 10 days of 3D cultures, we observed a higher ratio of CLL to FRCs compared with that of leukemia and FRCs in 2D, suggesting that the 3D structure of spheroids maintains a homeostatic equilibrium in culture, resulting in a more physiological ratio of cell subsets (Figure 2B) without cellular overgrowth.

To assess the viability of leukemic cells, we performed Annexin-V/propidium iodide (PI) flow cytometry analysis at 96 h and compared 2D and 3D conditions. We confirmed that the viability of CLL cells

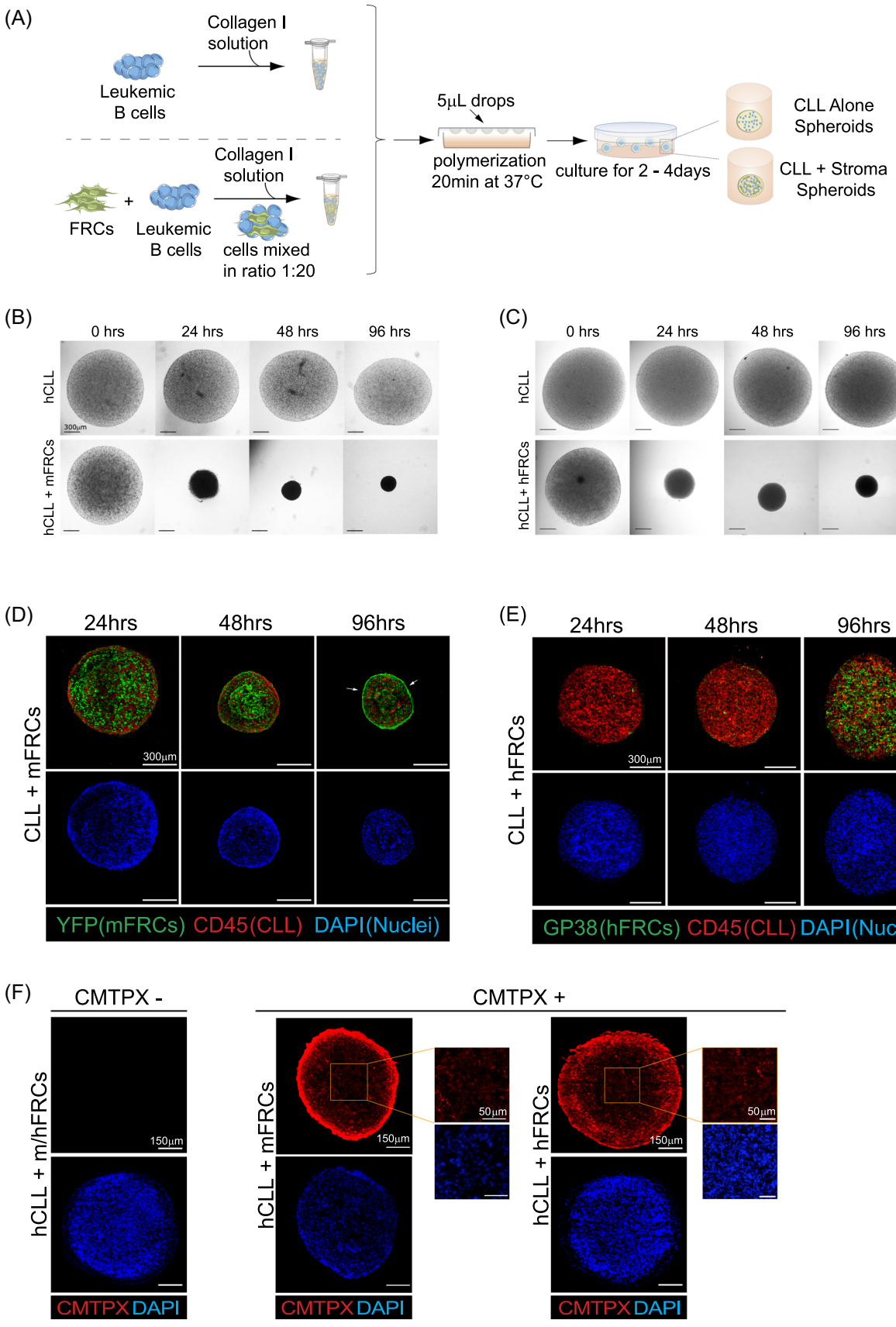

FIGURE 1 (See caption on next page).

FIGURE 1 **Dynamic of spheroids formation, cells positioning, and dye perfusion. (A)** Experimental design of spheroids formation. Human leukemic cells from chronic lymphocytic leukemia (CLL) patients were mixed or not along with a murine splenic fibroblastic reticular cell (FRC) line YFP$^+$ or a human lymph node-derived FRC line in a rat tail Collagen I solution. Droplets of the resulting cell suspensions were spotted on the lids of Petri dishes and placed in an incubator at 37°C to allow collagen polymerization. After 20 min, droplets were flushed into the medium by gentle pipetting, and CLL alone or CLL + FRCs spheroids were cultured for 2–4 days. **(B, C)** Representative bright field images of spheroids with CLL cells alone (upper panel) or with murine **(B)** or human **(C)** FRCs (lower panel), at different incubation periods, 24, 48, and 96 h, after spheroids preparation. Scale bar: 300 µm. **(D, E)** Confocal images of spheroids stained for YFP or PDPN (green) and CD45 (red) to detect murine or human FRCs and leukemic cells, respectively, and nuclei (blue) were stained with DAPI. Three time points after culture (24, 48, and 96 h) are shown. Scale bar: 300 µm. **(F)** Representative fluorescence image of CLL + murine/human FRC spheroids perfused with CMTPX Cell Tracker™, after 12 h of incubation with the dye. 4',6-diamidino-2-phenylindole (DAPI) staining (in blue) was performed to stain nuclei. Scale bars: 150 and 50 µm.

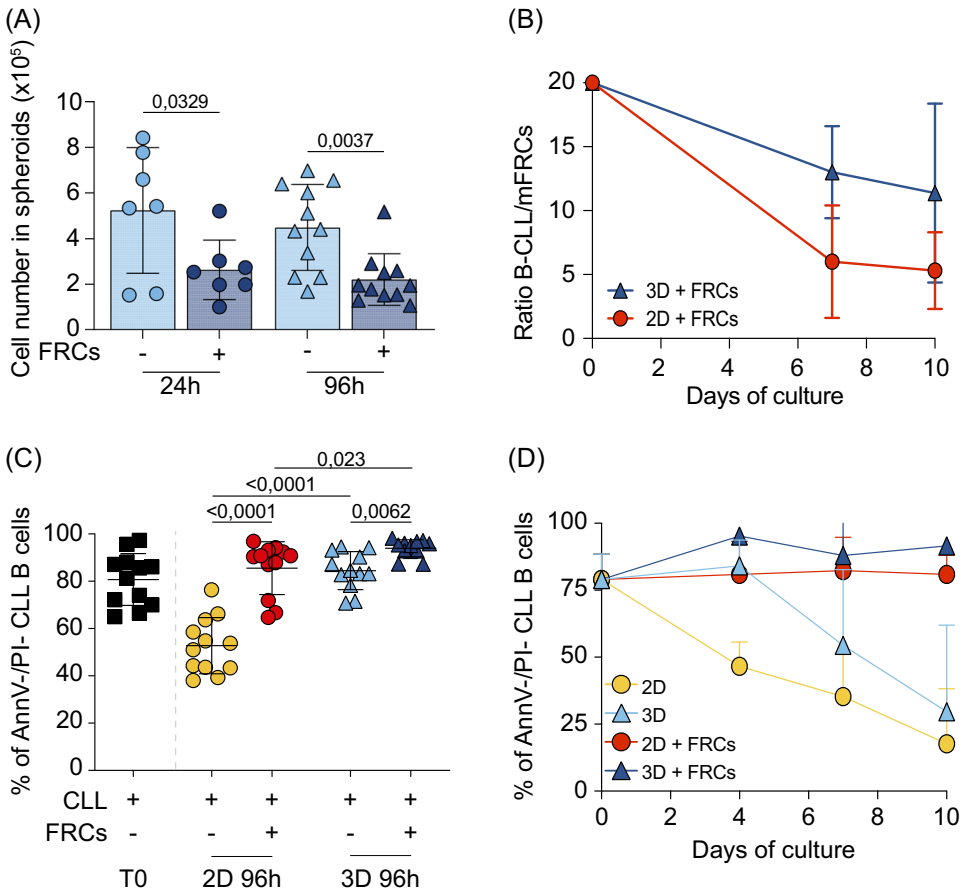

FIGURE 2 **Spheroids support chronic lymphocytic leukemia (CLL) viability. (A)** Analysis of the CLL B cell number in spheroids over time at two different time points (24 and 96 h), for both culture settings (CLL alone and CLL + murine fibroblastic reticular cells [FRCs]). A pool of three spheroids was prepared and digested to obtain a cell suspension. Then, cells were placed in the Bürker chamber and manually counted. Trypan Blue was added to exclude dead cells. Data are representative of CLL cells from 7 to 11 different patients cultured for 24–96 h, respectively. **(B)** Graph showing the differences in the cell ratio between the 2D and 3D conditions in the presence of murine FRCs. The ratio is calculated as the total number of CLL cells over the total number of FRCs at two different time points (7 and 10 days). Data are plotted as mean ± SD of four independent experiments/CLL samples. **(C, D)** Test of cell viability at short-term **(C)** and long-term **(D)** spheroid culture. Graphs show cell viability as a percentage of Annexin-V/propidium iodide (PI) double negative cells at 4 days **(C, D)** and at 7–10 days of culture **(D)**. Data are representative of 12 independent experiments for short-term culture **(C)** and 5 independent experiments for long-term culture **(D)**. Data are represented as mean ± SD.

cultured in 2D with FRCs was improved compared to traditional 2D cultures in the absence of FRCs and, interestingly, was equivalent to the viability of CLL cells cultured in 3D alone.

The latter result suggests that the 3D configuration, together with the presence of an FRCs-derived ECM protein such as collagen, may mimic the effect produced by stromal signals in a 2D environment (Figure 2C). Consistent with this, we observed the highest viability when CLL cells were cultured in a 3D configuration with FRCs compared with 2D cultures (Figure 2C).

Moreover, 3D spheroids generated with FRCs showed the greatest homogeneity in terms of cell viability across experiments and patients, as values were mostly close to 90%–95%, whereas values for all other conditions were more scattered and heterogeneous (Figure 2C). In particular, in long-term cultures (10 days), the viability of CLL cells cultured alone in 2D or 3D gradually decreased until only 20%–25% of cells were viable at the end of the culture period (Figure 2D).

In contrast, CLL cells cultured in 3D with FRCs showed a slight but nonsignificant increase in viability compared with cells cultured in

2D in the presence of FRCs. Interestingly, the viability of leukemic cells at Day 10 was also slightly higher than that of cells before culture (T0), suggesting that stroma-derived signals, together with the 3D geometric structure of spheroids, may have prevented some CLL cells from undergoing apoptosis (Figure 2D). These results suggest that spheroids maintain physiological cell ratios and promote CLL cell survival better than conventional 2D culture systems.

The spheroid microenvironment protects leukemic cells from drug effects

It is well described that cancer cells cultured in 3D spheroids are more resistant to anticancer drugs compared to 2D monolayers. However, limited data are available for hematologic cancers in this context.[27–29] To assess whether the 3D spheroids we generated could be better predictive of drug efficacy, we selected two Food and Drug Administration-approved drugs for CLL treatment, ibrutinib (Brüton's tyrosine kinase inhibitor) and venetoclax (BCL2 inhibitor).[2]

We first assessed the viability of leukemic cells after ibrutinib treatment and compared it with cells cultured in 2D in the presence or absence of murine FRCs. After 96 h, cells from 2D and 3D settings were collected, processed to obtain a single cell suspension, and stained with Annexin-V/PI (Figure S1B). The analysis revealed that ibrutinib treatment induced a modest but still significant apoptosis of leukemic cells cultured alone in 2D, whereas the percentage of apoptotic cells decreased significantly in the presence of murine FRCs (Figure S1). In 3D settings, apoptosis of leukemic cells cultured alone was significantly reduced compared with the same 2D conditions (Figure 3B). However, treatment of leukemic cells in 3D in the presence of FRCs did not significantly affect apoptosis when compared with the control vehicle, though we found that ibrutinib-treated spheroids contained fewer cells than vehicle-treated spheroids (Figure S1B). These findings indicate that ibrutinib treatment per se did not affect cell viability in 3D after 72 h treatment, and this is consistent with the observation that ex vivo it shows mainly an antiproliferative effect, with only a minor reduction of cell viability.[30]

We next compared the effect of venetoclax treatment in spheroids generated with murine or human FRCs. As expected, we found that treatment in 2D cultures severely impaired cell viability, both when CLL cells were cultured alone and with FRCs, though human FRCs showed a more protective effect compared to murine FRCs (Figure 3B,C).

However, the percentage of apoptotic cells in 3D in the presence of murine or human FRCs decreased significantly compared with 2D, and as expected, it was not abrogated by the 3D culture setting (Figure 3B,C). Although venetoclax-treated spheroids containing murine FRCs exhibited a reduced presence of CLL cells compared to spheroids generated with human FRCs, the immunofluorescence analysis did not reveal significant changes in cell distribution or density (Figure 3D,E). Taken together, these results suggest that the 3D environment is protective compared with conventional 2D cultures and that the presence of FRCs in this context further increases this effect, particularly when compared to conventional 2D cultures.

Gene signatures of CLL cells in spheroids mimic those in LNs

Having established that the 3D spheroid model recapitulates some of the protective effects of the lymphoid microenvironment, as those observed in spleen and LNs, we next evaluated whether CLL cells in 3D change their transcriptomic profile compared to that of cells cultured in a 2D setting. To address this, we isolated CLL cells from the 3D and 2D models generated in the presence of human FRCs and performed bulk RNA sequencing (Figure 4A).

Principal component analysis (PCA) revealed a clear separation between CLL cells from 2D and 3D conditions, primarily along the first principal component (PC1), indicating that the model significantly contributes to the overall transcriptional variance in the dataset (Figure 4B).

We then performed differential gene expression analysis and identified 467 downregulated genes and 240 upregulated genes in CLL cells cultured in 3D culture compared to cells the 2D culture with adjusted P-value < 0.05 and $|\log FC| > 1$ (Figure 4C).

Gene ontology revealed that CLL cells in the 3D microenvironment upregulated genes related to cell–cell adhesion, matrix organization, and hypoxia, which likely reflect the more physiological nature of the 3D setting compared to the 2D culture (Figure 4D). Interestingly, in the 3D versus 2D comparison, we observed an upregulation of genes associated with the interferon response, toll-like receptor signaling, regulation of B-cell activation, and cytokine signaling, indicating a LN-like behavior of CLL cells. In contrast, genes associated with cell–cell junctions and focal adhesion were upregulated in 2D cultures, reflecting the organization of cells in conventional 2D culture.

Importantly, we found that in the 3D environment, the expression of antiapoptotic genes such as *BCL2*, *BCL2L11*, and *MCL1* was upregulated, whereas the proapoptotic genes *BAX* and *BAD* were more highly expressed in the 2D setting (Figure 4E).

Together, these findings suggest that the 3D microenvironment promotes a gene expression profile that closely resembles that of CLL cells in their natural physiological environment, such as within the LN, and suggests that the protective effect observed in the 3D spheroid model is, at least in part, driven by the induction of antiapoptotic genes.[6]

DISCUSSION

Currently, 3D culture systems capable of accurately mimicking the complex spatial and cellular organization of the CLL microenvironment, which is essential for evaluating drug efficacy, are still limited. Therefore, the development of a more physiological in vitro 3D system that mimics the features of the natural lymphoid microenvironment such as LN is needed. We have developed a spheroid model that enables FRC–leukemia interactions within a collagen-based microenvironment that mimics the ECM of lymphoid tissues. In conventional culture models, cells are in a 2D compartment and forced into a single flat interface, which hinders the ability to generate more complex and physiological interactions. In contrast, CLL cells in the spheroid model are not constrained in a single flat layer but interact more physiologically within the 3D surrounding microenvironment.

Our data show that a 3D system, with only a collagen-based matrix, is sufficient to replicate the native supportive microenvironment, as evidenced by the significantly enhanced viability of CLL cells compared to that of CLL cells kept under conventional 2D cultures and in the absence of supporting stroma. Leukemic cells may benefit from integrin-binding sites in the collagen matrix, which promote their survival, as reflected in the upregulation of genes associated with cell–cell adhesion and matrix organization. Interestingly, the gene expression profile of CLL cells in 3D also revealed similarities to that of CLL cells isolated from LNs, and these include signatures associated to B-cell activation and toll-like receptor and Nfkb signaling previously found expressed by CLL cells in the LN, indicating that the spheroid model better recapitulates the native microenvironment

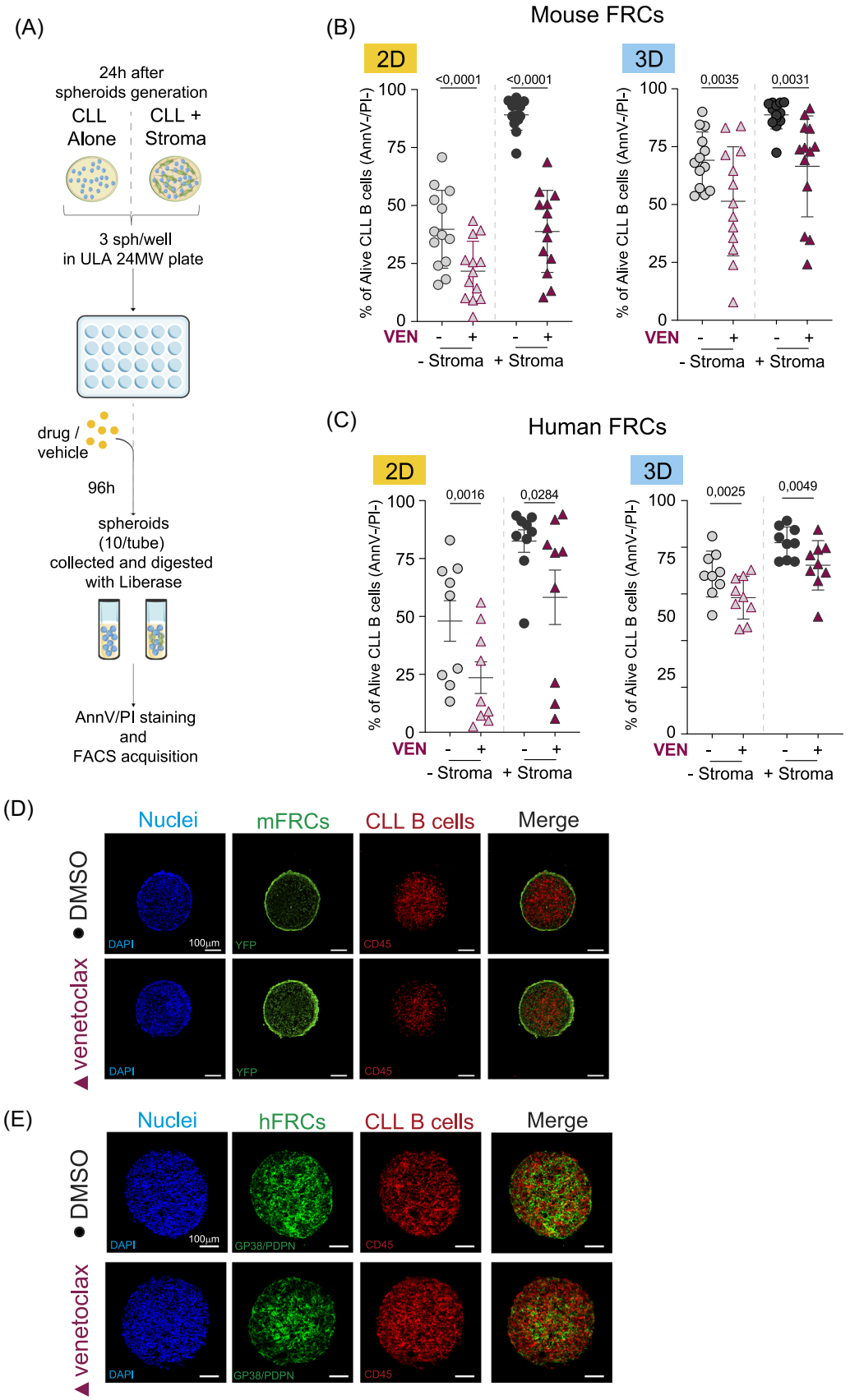

FIGURE 3 (See caption on next page).

FIGURE 3 **Spheroids protect from drug-induced apoptosis. (A)** Experimental scheme of spheroids treatment with drugs. After 24 h from spheroids generation, chronic lymphocytic leukemia (CLL) alone or CLL + murine or human fibroblastic reticular cell (FRC) spheroids were distributed in a 24-multiwell ultra-low attachment plate (3 spheroids/well) and were cultured for 96 h in presence of drug (ibrutinib or venetoclax) or vehicle (dimethyl sulfoxide [DMSO]). Then, spheroids were collected, randomly distributed in tubes (10 spheroids/tube), and digested with Liberase™ to obtain a single cell suspension. Next, samples were stained for Annexin-V and propidium iodide (PI) and analyzed by flow cytometry. **(B, C)** Graphs represent CLL cell viability at 72 h post-treatment with venetoclax in 2D (left) and 3D (right) conditions of spheroids generated with murine FRCs **(B)** or human FRCs **(C)**. Double negative CLL cells for Annexin-V/PI staining are shown as percentages of total cells. Data are representative of 13 samples and are plotted as mean ± SD. **(D, E)** Representative confocal microscope images of spheroids prepared with CLL B cells and murine FRCs **(D)** or human FRCs **(E)** treated for 72 h with venetoclax or vehicle (DMSO). Antibodies against YFP **(D)** protein or PDPN **(E)** (green), to mark the FRC population, and hematopoietic superficial marker CD45 (red), for CLL cells, were used. 4',6-diamidino-2-phenylindole (DAPI) staining (blue) was performed to stain nuclei. Scale bar: 100 μm.

through physiological interactions.[6] The 3D spheroid model allows efficient nutrient diffusion to the interior, which is supported by previous reports showing that collagen-based hydrogels facilitate the exchange of oxygen, waste, and nutrients within spheroids during both short- and long-term cultures.[31]

The viability of CLL cells in 3D is high even if our gene expression analysis revealed upregulation of hypoxia-related genes compared to 2D cultures, and this hypoxic microenvironment reflects features observed in normal LN.[32]

Furthermore, the viability of leukemic cells is significantly enhanced by the presence of FRCs, with the effect being even more pronounced in 3D cultures. Leukemic cells can no longer survive independently unless continuously supported by an appropriate microenvironment, such as that provided by FRCs. This is consistent with the role of FRCs in promoting CLL cell survival, where interactions between FRCs and CLL cells, via integrin VLA-4 binding to VCAM-1 on FRCs, lead to upregulation of antiapoptotic proteins like BCL2 and MCL1, which we also found upregulated in 3D compared to 2D.[8,33] Additionally, the presence of FRCs in our spheroids resulted in a shrinkage of the spheroid diameter over time, due to the tensile forces generated by FRC contraction. This suggests that FRCs in the 3D model behave similarly to in vivo, where they play a crucial role in controlling LN swelling during immune responses or in the resolution phase of inflammation.[31,33]

Consistent with this, during spheroid formation, we observed a gradual increase in PDPN expression, which is known to regulate the contraction of FRCs in LNs.

It is important to note that the 3D culture system maintains a higher ratio of FRCs to leukemic cells than 2D cultures, where FRCs tend to proliferate and overgrow, deviating from the in vivo balance. This also highlights the advantage of the 3D model in more closely mimicking the physiological conditions for all the cellular components involved.

Our results suggest that spheroids recapitulate the interactions that occur in vivo between CLL cells, the ECM, and FRCs by promoting active stroma–leukemia crosstalk, even when drugs are administered. Although the response to ibrutinib and venetoclax in our model was not as pronounced as expected, it is important to note that these drugs induce apoptosis in vivo in CLL patients over a longer period of time, and the efficacy appears to be more limited in the disease present in the LNs. Though this protective effect may represent a limitation of our system, the results are likely reflective of a shorter treatment duration which may not fully capture the drug's long-term effects observed in vivo, it is also relevant to speculate that our 3D model is providing more protection toward the cytotoxic effect of the drugs, paralleling the evidence in patients where the LNs > 5 cm are predictive of a shorter clinical response.

These findings were corroborated using mouse and human FRCs, indicating that, although less physiological, the use of murine cells when human FRCs are not available could also be a valid alternative. At present, our model has not been tested for assessing the behavior and response to drugs of CLL cells from patients with different clinical courses and genetic alterations, and additional work is needed to further explore the use of this 3D spheroid model to predict clinically relevant responses. Nevertheless, we envision that our 3D spheroid model could be integrated into an automated process, as it requires minimal standard equipment and reagents for fabrication. These characteristics align with the current demands of HTS in 3D drug development, making this spheroid model an attractive platform for CLL research and other B-cell malignancies.

Key resources table

Reagent or resource	Source	Identifier
Primary antibodies		
Anti-chicken GFP	Abcam	Cat# ab13970 RRID: AB_300798
Anti-human CD45 PE	Biolegend	Cat# 304008 RRID: AB_314396
Anti-human CD45 biotinylated	Biolegend	Cat# 304004 RRID: B_314392
Anti-human CD19 APCCy7	Biolegend	Cat# 302218 RRID: AB_314248
Anti-human CD5APC	Biolegend	Cat# 300612 RRID: AB_314098
Annexin-V APC	BD	Cat# 550475 RRID: AB_2868885
Anti-human PDPN/GP38 purified	Biolegend	Cat# 337002 RRID: AB_1595511
Secondary antibodies		
Anti-chicken Alexa Fluor 488	Thermo Fisher Scientific	Cat# A11039 RRID: AB_142924
Anti-rat Alexa Fluor 488	Thermo Fisher Scientific	Cat# 21208 RRID: AB_141709
Streptavidin Alexa Fluor 546	Thermo Fisher Scientific	Cat# S11225 RRID: AB_2532130
Reagents		
DMEM	Gibco	Cat# 41966-029
RPMI 1640 medium GlutaMAX™	Gibco	Cat# 61870-010
FBS	Euroclone	Cat# ECS5000L
2.5% Trypsin	Gibco	Cat# 15090-046
Pen/Strep	Gibco	Cat# 15140-122

(Continues)

Reagent or resource	Source	Identifier
L-Glutammine	Gibco	Cat# 25030-024
Sodium pyruvate	Gibco	Cat# 11360-039
Nonessential amino acids (NEAA)	Gibco	Cat# 11140-035
PBS 1×	Corning	Cat# 21-031-CV
NaOH	Sigma	Cat# 71608
RosetteSep B lymphocyte enrichment kit	StemCell Technologies	Cat# 15024
Rat tail Collagen I	Corning	Cat#354236
Cell Tracker™ Red CMTPX Dye	Life Technologies	Cat# C34552
24-Well multiwell plate Ultra-Low Attachment	Corning	Cat# 10327701
Annexin Buffer	Biolegend	Cat# 79998
Cell Staining Buffer	Biolegend	Cat# 420201
Chemicals, peptides, and recombinant proteins		
Antigenfix	Diapath	Cat# P0014
Killik (O.C.T.)	Bio-Optica	Cat# 05-9801
Dehyol 95	Bio-Optica	Cat# 06-10070Q
Avidin/Biotin Blocking Kit	Vector Laboratories	Cat# SP-2001
M.O.M.® Blocking Reagent	Vector Laboratories	Cat# MKB-2213-1
DAPI	Sigma-Aldrich	Cat# 32670
MOWIOL® 4-88 Reagent	Merck	Cat# 475904-M
Liberase™	Roche	Cat# 05401119001
Ibrutinib	Aurogene	Cat# S2680
Venetoclax	MedChemExpress	Cat# HY-15531
DMSO	Sigma	Cat# D8418
PI	BD	Cat# 51-66211E
Software and algorithms		
Prism 7.0	GraphPad	
FlowJo V10	TreeStar	
ImageJ V1.5	ImageJ	
Adobe Illustrator CC 2022	Adobe	
Leica Application Suite X (LAS X)	Leica Microscope	
Other		
FC500	Beckman Coulter	
Cytoflex S	Beckman Coulter	
SP8 confocal microscope	Leica Microsystem	
Axio Observer	Leica Microsystem	

Materials availability

This study did not generate new unique reagents.

Methods

Human samples

Human primary samples were obtained from CLL patients at Rai Stages 0–1 after obtaining institutional committee approval (protocol VIVI-CLL) from the San Raffaele Scientific Institute (Milan, Italy) in accordance with the Declaration of Helsinki.

FRCs and human CLL B cells

A mouse spleen-derived stromal cell (mSSC) line expressing YFP was generated as previously described, or an LN-derived human FRC line was used.[14] Cells were cultured at 37°C, 5% CO_2 in RPMI (Gibco) supplemented with 10% heat-inactivated fetal bovine serum (FBS; Euroclone), 2 mM L-glutamine (L-Glu; Gibco), 100 U/mL penicillin, and 100 µg/mL streptomycin (Pen/Strep; Gibco). All cell lines were tested monthly for mycoplasma.

Human CLL cells were purified immediately after blood collection by negative depletion using the RosetteSep B lymphocyte enrichment kit (StemCell Technologies). The purity of all human preparations was always greater than 99%, and cells expressed CD19 and CD5 on their cell surface as tested by flow cytometry (FC500; Beckman Coulter); preparations were virtually free of natural killer cells, T lymphocytes, and monocytes. Human primary samples were obtained from CLL patients at Rai Stages 0–1 after obtaining institutional committee approval (Protocol ViVi-CLL) from the San Raffaele Scientific Institute (Milan, Italy) in accordance with the Declaration of Helsinki. Human purified CLL B cells were either used immediately as fresh samples or frozen with 10% dimethyl sulfoxide (DMSO) in FBS until use. CLL B cells were cultured at 37°C, 5% CO_2 in complete RPMI 1640 medium GlutaMAX™ supplemented with 10% heat-inactivated FBS (Euroclone), 2 mM L-Glu (Gibco), 100 U/mL penicillin (Gibco), 100 µg/mL streptomycin (Gibco), MEM nonessential amino acids solution 1× (Gibco), and sodium pyruvate 1 mM (Gibco).

Cell cultures, spheroids preparation, and analyses

For 2D cultures, 8×10^5 human leukemic B cells were mixed alone (monoculture) or together with 4×10^4 immortalized FRCs (coculture) at a ratio of 20:1 and seeded in 48 multiwell plates (Costar, Corning). Human leukemic B cells and FRCs were also used for spheroid formation (3D culture). Specifically, for each spheroid, CLL B cells and FRC cells were mixed at a ratio of 20:1 (4×10^5 and 2×10^4 cells for each aggregate, respectively), pelleted, and resuspended in 0.9% type I rat tail collagen solution as previously published.[34] Briefly, 500 µL of collagen solution was prepared on ice with the following components: 342 µL of Dulbecco's modified Eagle medium (DMEM), 15 µL of phosphate-buffered saline (PBS) 10×, 3 µL of NaOH 1 M (Sigma), and 140 µL of rat tail Collagen I (#354 236; Corning) and used immediately after preparation. Five-microliter drops of the resulting cell suspension were spotted as hanging drops on the lid of a Petri dish and incubated in a humidified incubator with 5% CO_2 at 37°C for 20 min to promote collagen polymerization. The polymerized droplets

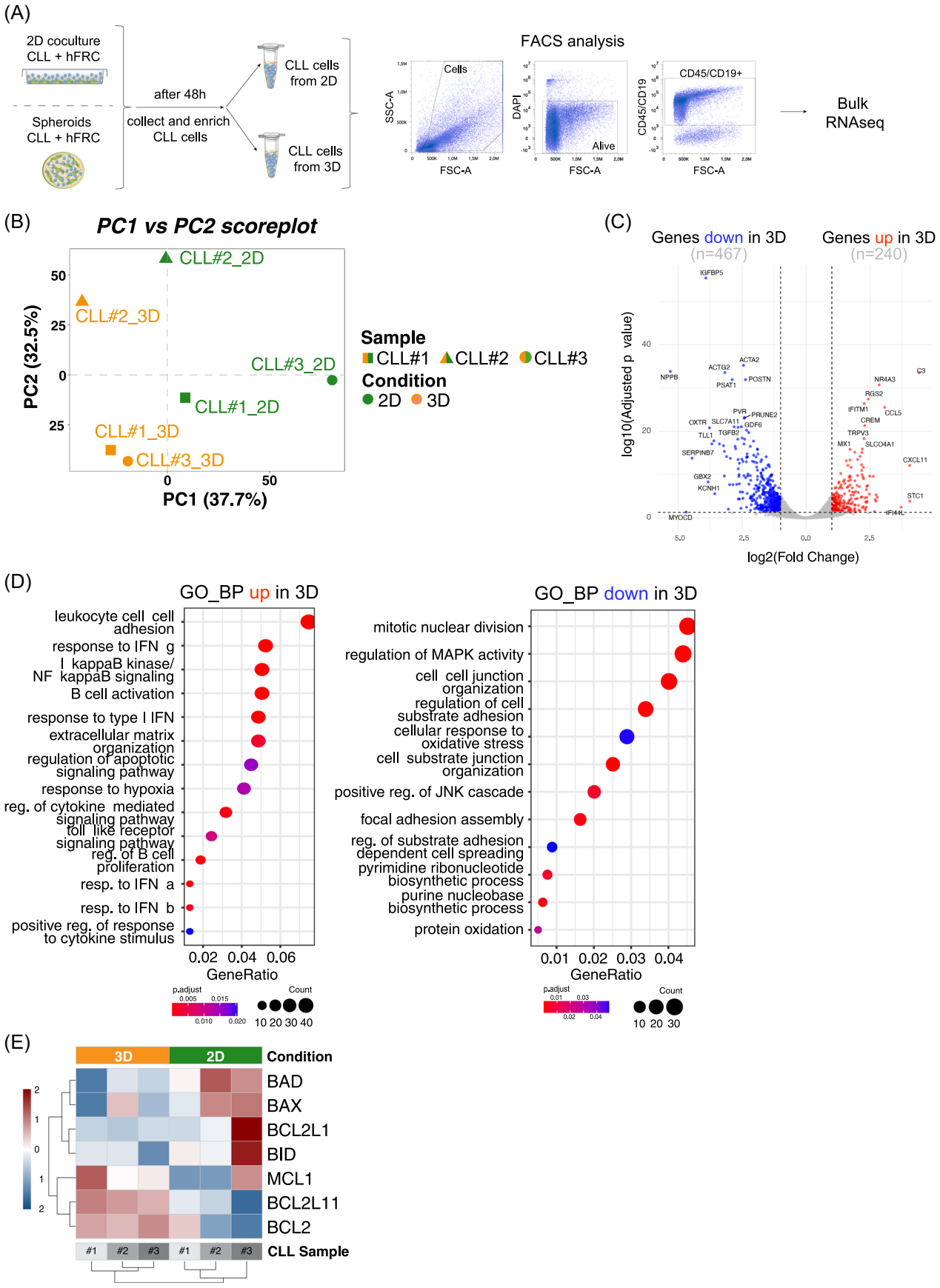

FIGURE 4 (See caption on next page).

FIGURE 4 **Gene expression profile of chronic lymphocytic leukemia (CLL) cells from 3D or 2D culture conditions. (A)** Experimental scheme of spheroids formation, CLL isolation, and flow cytometry gating strategy. **(B)** Principal component analysis of 5000 most variable genes (log 10 rpkm) in bulk RNA-seq samples from 3D and 2D spheroids. **(C)** Volcano plot of differentially expressed genes (DEGs) in 3D versus 2D spheroids. Significantly upregulated genes in the 3D spheroids are highlighted in red, downregulated in blue (|log FC| > 1, adjusted P-value < 0.05). Nonsignificant genes are displayed in gray. **(D)** Dot plot of selected significant (adjusted P-value < 0.05) Gene Ontology (GO) Biological Process (BP) pathways for upregulated and downregulated DEGs. **(E)** Hierarchically clustered heatmap (*Z* score) of apoptotic and antiapoptotic gene expression in 3D and 2D spheroids.

were then transferred to a Petri dish containing complete growth medium. After 24 h, the organoids were fully formed by the contraction of collagen[35] and could be used for further characterization, permeability testing, or drug treatment experiments.

For the permeability assay, spheroids were incubated for 12 h with 7.5 μM Cell Tracker™ Red CMTPX Dye (Life Technologies) solution prepared according to the manufacturer's protocol. Spheroids were then harvested, cryosectioned, and slices mounted with Mowiol for further confocal microscope analysis.

For assessing cell numbers inside spheroids, pooled spheroids ($n = 5–7$) were collected and digested in 60 μL of Liberase solution (0.3 mg/mL in FBS) at 37°C in a thermomixer at 1000 rpm until spheroids were completely dissolved and then washed in complete media.

Aliquots from the resulting cell suspension were diluted to a 1:2 ratio in Trypan Blue (Sigma), and cells were counted by using a Burker's chamber with a phase contrast Olympus CK2 inverted microscope.

For drug test, a pool of three spheroids was placed in a 24-multiwell ultra-low attachment plate (Corning) and treated with Ibrutinib (1 μM) or venetoclax (5 nM), dissolved in DMSO, and incubation was extended for 72 h. Spheroids were then collected and processed for further flow cytometry or immunofluorescence analyses.

FACS analysis

Pools of 3–5 spheroids were collected, washed with PBS 1×, and digested with 0.3 mg/mL of Liberase™ (Roche) in FBS at 37°C for 15–20 min in a thermomixer at 900 rpm. Then, the resulting cell suspension was centrifuged at 1500 rpm for 5 min, and the cell pellet was resuspended in 0.2% FBS in Annexin buffer (Biolegend). For viability analysis, cells were incubated with 3.5 μL of Annexin V–APC conjugated antibody (BD #550 475) for 10 min in the dark at RT, then centrifuged and finally resuspended in 300 μL of Annexin buffer. Immediately before imaging, 8 μL of PI (BD) was added to each sample. Data were acquired using FC500 or CytoflexS flow cytometer (both from Beckman Coulter) and analyzed using FlowJo v10.6.2 (TreeStar, Ashland, OR, USA).

Immunofluorescence staining

Spheroids were collected, washed 1× in PBS, and fixed with Antigen Fix (Diapath) for 5 min at RT. Samples were embedded in Tissue-Tek OCT (Bio-Optica), frozen in an ethanol dry ice bath (using Dehyol 95 from Bio-Optica), and stored at −80°C until use. Eight-micrometer-thick sections were placed on glass slides (Thermo Fisher Scientific), fixed in ice-cold acetone (Sigma-Aldrich) for 5 min, dried, and stored at −80°C until used.

Slides were incubated for 30 min at RT with a blocking solution of PBS containing 0.5% FBS and 0.05% Tween (VWR) (PBS-T 0.05%) and then incubated for 1 h with primary specific antibodies—biotinylated anti-human CD45 (1:20; Biolegend #304004) and anti-chicken GFP (1:250; Abcam #ab13970). Sections were then incubated for 30 min with streptavidin Alexa Fluor 546 and goat anti-chicken Alexa Fluor 488 secondary antibodies (both from Thermo Fisher Scientific). Cell nuclei were visualized with DAPI (Sigma-Aldrich) and fixed with Mowiol (Calbiochem). Confocal images were acquired using Leica TCS SP8 or Axio Observer microscopes. Digital images were acquired in separately sampled channels, with no overlap of emissions from the respective fluorochromes. Final image processing was performed using ImageJ and Adobe Illustrator 2023.

Sample preparation, RNA sequencing, and bioinformatic analysis

After 48 h from 2D cultures and spheroids preparation, CLL cells were collected by digestion or with trypsin as previously described and enriched with anti-GP38 coated plates. After 45 min of incubation, CLL cells were collected and purity (> 98%) was tested by flow cytometry. RNA was extracted using the RNeasy Mini Isolation Kit (Qiagen) according to the manufacturer's protocol. RNA-Seq libraries were prepared using the Illumina TruSeq Stranded mRNA Kit. Sequencing was performed in PE mode on an Illumina NovaSeq 6000 instrument (Illumina, San Diego, CA) according to the manufacturer's recommendations. Paired-end reads (100 bp) were trimmed with Trimmomatic (v0.39)[36] to remove adapters and exclude low-quality reads from the analysis and aligned to the GRCh38 reference genome using the STAR aligner (v2.5.3a).[37] FeatureCounts (v1.6.4)[38] was used to compute reads mapping on exons as annotated in GENCODE human basic gene annotation (v 31) and obtain transcript quantification summarized at the gene level, excluding multimapping reads.

Only genes with at least 1 CPM (counts per million) in at least three samples were retained. Differential gene expression analysis was performed with DESeq2[39] bioconductor library (v1.30.1). Hierarchically clustered heatmaps were made with Pheatmap[40] R package (v1.0.12). PCA was computed on the top 5000 most variable genes (log 10 rpkm) with DESeq2 Biocondutor package "plotPCA" and plotted with ggplot2 (v3.4.2)[41] "geom_point" function. Dot plots of significant pathways were generated with ClusterProfiler[42] R package (v4.3.0) on differentially expressed genes (DEGs with |log FC| > 0, adjusted P-value < 0.05). To minimize redundancy among pathways and enhance enrichment results interpretation, we plotted Jaccard distance heatmaps for each condition using all pathways from the GO_Biological_Process_2023 dataset with an adjusted P-value < 0.01. GSEA enrichments were performed with clusterProfiler using GSEA C2 and C5 gene sets and graphically represented with enrichplot (v1.10.2). RNA-sequencing data have been deposited at GEO and will be available through the accession number GSE299467.

Quantification and statistics

Data were analyzed using GraphPad Prism 7 (GraphPad Software Inc). To assess statistical differences between samples, a two-sided, unpaired Student's test was performed. *P < 0.05, **P < 0.01, ***P < 0.001, and ****P < 0.0001. All data are presented as means ± SD. Group sizes were estimated based on pilot studies to determine success rate and reproducibility.

ACKNOWLEDGMENTS

The authors are grateful to lab members for technical assistance and helpful suggestions. Open access funding provided by BIBLIOSAN.

AUTHOR CONTRIBUTIONS

Elisa Lenti: Conceptualization; investigation; methodology; validation; data curation; writing—review and editing; formal analysis. **Edoardo Visentin**: Conceptualization; data curation; investigation; methodology; validation; writing—review and editing; formal analysis. **Engin Bojnik**: Conceptualization; data curation; methodology; investigation; validation; formal analysis. **Alessia Neroni**: Data curation; investigation; methodology; validation; formal analysis. **Martina Franchino**: Data curation; investigation; validation; formal analysis; writing—review and editing. **Daniela Talarico**: Writing—review and editing; conceptualization. **Nicolò Sacchetti**: Conceptualization; methodology. **Lydia Scarfò**: Investigation; methodology; resources. **Aurora Maurizio**: Data curation; methodology; investigation; writing—review and editing; conceptualization. **Jose Manuel Garcia-Manteiga**: Investigation; methodology; writing—review and editing; data curation; conceptualization. **Paolo Ghia**: Conceptualization; data curation; writing—original draft; writing—review and editing; supervision; funding acquisition; resources. **Andrea Brendolan**: Conceptualization; data curation; writing—original draft; writing—review and editing; methodology; investigation; supervision; funding acquisition.

CONFLICT OF INTEREST STATEMENT

Paolo Ghia reported the following conflicts of interest: Research funding from AbbVie, AstraZeneca, BMS, and Janssen. Honorarium from AbbVie, AstraZeneca, BeiGene, BMS, Janssen, Loxo@Lilly, MSD, and Roche.

DATA AVAILABILITY STATEMENT

The data that support the findings of this study are available from the lead contact, Andrea Brendolan, upon reasonable request.

FUNDING

This work was supported by Associazione Italiana Ricerca sul Cancro (AIRC) Grants ID 19867 and 27174 to Andrea Brendolan; AIRC under 5 per Mille 2018—ID 21198 to P. I. Foà Roberto, G. L. Ghia Paolo, and ID 27566 to Ghia Paolo.

ORCID

Paolo Ghia https://orcid.org/0000-0003-3750-7342
Andrea Brendolan https://orcid.org/0000-0003-0109-6879

SUPPORTING INFORMATION

Additional supporting information can be found in the online version of this article.

REFERENCES

1. Caligaris-Cappio F, Hamblin TJ. B-cell chronic lymphocytic leukemia: a bird of a different feather. *J Clin Oncol*. 1999;17:399. doi:10.1200/JCO.1999.17.1.399
2. Jain N, Keating M, Thompson P, et al. Ibrutinib and venetoclax for first-line treatment of CLL. *N Engl J Med*. 2019;380:2095-2103. doi:10.1056/NEJMoa1900574
3. Al-Sawaf O, Robrecht S, Zhang C, et al. Venetoclax–obinutuzumab for previously untreated chronic lymphocytic leukemia: 6-year results of the randomized phase 3 CLL14 study. *Blood*. 2024;144:1924-1935. doi:10.1182/blood.2024024631
4. Apollonio B, Ioannou N, Papazoglou D, Ramsay AG. Understanding the immune-stroma microenvironment in B cell malignancies for effective immunotherapy. *Front Oncol*. 2021;11:626818. doi:10.3389/fonc.2021.626818
5. Caligaris-Cappio F, Bertilaccio MTS, Scielzo C. How the microenvironment wires the natural history of chronic lymphocytic leukemia. *Sem Cancer Biol*. 2014;24:43-48. doi:10.1016/j.semcancer.2013.06.010
6. Dadashian EL, McAuley EM, Liu D, et al. TLR signaling is activated in lymph node-resident CLL cells and is only partially inhibited by ibrutinib. *Cancer Res*. 2019;79:360-371. doi:10.1158/0008-5472.CAN-18-0781
7. Ghia P, Caligaris-Cappio F. The indispensable role of microenvironment in the natural history of low-grade B-cell neoplasms. *Adv Cancer Res*. 2000;79:157-173. doi:10.1016/s0065-230x(00)79005-1
8. Herishanu Y, Katz BZ, Lipsky A, Wiestner A. Biology of chronic lymphocytic leukemia in different microenvironments. *Hematol Oncol Clin North Am*. 2013;27:173-206. doi:10.1016/j.hoc.2013.01.002
9. Svanberg R, Janum S, Patten PEM, Ramsay AG, Niemann CU. Targeting the tumor microenvironment in chronic lymphocytic leukemia. *Haematologica*. 2021;106:2312-2324. doi:10.3324/haematol.2020.268037
10. ten Hacken E, Burger JA. Microenvironment dependency in chronic lymphocytic leukemia: the basis for new targeted therapies. *Pharmacol Ther*. 2014;144:338-348. doi:10.1016/j.pharmthera.2014.07.003
11. Acton SE, Onder L, Novkovic M, Martinez VG, Ludewig B. Communication, construction, and fluid control: lymphoid organ fibroblastic reticular cell and conduit networks. *Trends Immunol*. 2021;42:782-794. doi:10.1016/j.it.2021.07.003
12. Bagdi E, Krenacs L, Krenacs T, Miller K, Isaacson PG. Follicular dendritic cells in reactive and neoplastic lymphoid tissues: a re-evaluation of staining patterns of CD21, CD23, and CD35 antibodies in paraffin sections after wet heat-induced epitope retrieval. *Appl Immunohistochem Mol Morphol*. 2001;9:117-124. doi:10.1097/00129039-200106000-00003
13. Buckley CD, Barone F, Nayar S, Bénézech C, Caamaño J. Stromal cells in chronic inflammation and tertiary lymphoid organ formation. *Annu Rev Immunol*. 2015;33:715-745. doi:10.1146/annurev-immunol-032713-120252
14. Castagnaro L, Lenti E, Maruzzelli S, et al. Nkx2-5(+)islet1(+) mesenchymal precursors generate distinct spleen stromal cell subsets and participate in restoring stromal network integrity. *Immunity*. 2013;38:782-791. doi:10.1016/j.immuni.2012.12.005
15. Lenti E, Genovese L, Bianchessi S, et al. Fate mapping and scRNA sequencing reveal origin and diversity of lymph node stromal precursors. *Immunity*. 2022;55:606-622.e6. doi:10.1016/j.immuni.2022.03.002
16. Panocha D, Roet JEG, Kuipers JE, de Winde CM, Mebius RE. Lymph node fibroblast-produced extracellular matrix shapes immune function. *Trends Immunol*. 2025;46:229-243. doi:10.1016/j.it.2025.02.002
17. Thierry GR, Gentek R, Bajenoff M. Remodeling of reactive lymph nodes: dynamics of stromal cells and underlying chemokine signaling. *Immunol Rev*. 2019;289:42-61. doi:10.1111/imr.12750
18. Wang X, Cho B, Suzuki K, et al. Follicular dendritic cells help establish follicle identity and promote B cell retention in germinal centers. *J Exp Med*. 2011;208:2497-2510. doi:10.1084/jem.20111449
19. Barozzi D, Scielzo C. Emerging Strategies in 3D culture models for hematological cancers. *HemaSphere*. 2023;7:e932. doi:10.1097/HS9.0000000000000932
20. Bruce A, Evans R, Mezan R, et al. Three-dimensional microfluidic tri-culture model of the bone marrow microenvironment for study of acute lymphoblastic leukemia. *PLoS One*. 2015;10:e0140506. doi:10.1371/journal.pone.0140506
21. Mannino RG, Santiago-Miranda AN, Pradhan P, et al. 3D microvascular model recapitulates the diffuse large B-cell lymphoma

tumor microenvironment in vitro. *Lab Chip*. 2017;17:407-414. doi:10.1039/c6lc01204c
22. Tian YF, Ahn H, Schneider RS, et al. Integrin-specific hydrogels as adaptable tumor organoids for malignant B and T cells. *Biomaterials*. 2015;73:110-119. doi:10.1016/j.biomaterials.2015.09.007
23. Antoni D, Burckel H, Josset E, Noel G. Three-dimensional cell culture: a breakthrough in vivo. *Int J Mol Sci*. 2015;16:5517-5527. doi:10.3390/ijms16035517
24. Fang Y, Eglen RM. Three-dimensional cell cultures in drug discovery and development. *SLAS Discov*. 2017;22:456-472. doi:10.1177/1087057117696795
25. Kunz-Schughart LA, Freyer JP, Hofstaedter F, Ebner R. The use of 3-D cultures for high-throughput screening: the multicellular spheroid model. *SLAS Discov*. 2004;9:273-285. doi:10.1177/1087057104265040
26. Haselager MV, van Driel BF, Perelaer E, et al. In vitro 3D spheroid culture system displays sustained T cell-dependent CLL proliferation and survival. *HemaSphere*. 2023;7:e938. doi:10.1097/HS9.0000000000000938
27. Aljitawi OS, Li D, Xiao Y, et al. A novel three-dimensional stromal-based model for in vitro chemotherapy sensitivity testing of leukemia cells. *Leuk Lymphoma*. 2014;55:378-391. doi:10.3109/10428194.2013.793323
28. Bray LJ, Binner M, Körner Y, von Bonin M, Bornhäuser M, Werner C. A three-dimensional ex vivo tri-culture model mimics cell–cell interactions between acute myeloid leukemia and the vascular niche. *Haematologica*. 2017;102:1215-1226. doi:10.3324/haematol.2016.157883
29. Hsieh CH, Chen YD, Huang SF, Wang HM, Wu MH. The effect of primary cancer cell culture models on the results of drug chemosensitivity assays: the application of perfusion microbioreactor system as cell culture vessel. *BioMed Res Int*. 2015;2015:470283. doi:10.1155/2015/470283
30. Primo D, Scarfò L, Xochelli A, et al. A novel ex vivo high-throughput assay reveals antiproliferative effects of idelalisib and ibrutinib in chronic lymphocytic leukemia. *Oncotarget*. 2018;9:26019-26031. doi:10.18632/oncotarget.25419
31. Cui X, Hartanto Y, Zhang H. Advances in multicellular spheroids formation. *J R Soc Interface*. 2017;14:20160877. doi:10.1098/rsif.2016.0877
32. Schito L, Rey S. Hypoxia orchestrates the lymphovascular-immune ensemble in cancer. *Trends Cancer*. 2022;8:771-784. doi:10.1016/j.trecan.2022.04.008
33. Koopman G, Parmentier HK, Schuurman HJ, Newman W, Meijer CJ, Pals ST. Adhesion of human B cells to follicular dendritic cells involves both the lymphocyte function-associated antigen 1/intercellular adhesion molecule 1 and very late antigen 4/vascular cell adhesion molecule 1 pathways. *J Exp Med*. 1991;173:1297-1304. doi:10.1084/jem.173.6.1297
34. Farinello D, Woźińska M, Lenti E, et al. A retinoic acid-dependent stroma–leukemia crosstalk promotes chronic lymphocytic leukemia progression. *Nat Commun*. 2018;9:1787. doi:10.1038/s41467-018-04150-7
35. Zhu, Y. K., UMINO T., LIU X.D., et al. Contraction of fibroblast-containing collagen gels: initial collagen concentration regulates the degree of contraction and cell survival. *In Vitro Cell Dev Biol Anim*. 2001;37(1):10-16.
36. Bolger AM, Lohse M, Usadel B. Trimmomatic: a flexible trimmer for Illumina sequence data. *Bioinformatics*. 2014;30:2114-2120. doi:10.1093/bioinformatics/btu170
37. Dobin A, Davis CA, Schlesinger F, et al. STAR: ultrafast universal RNA-seq aligner. *Bioinformatics*. 2013;29:15-21. doi:10.1093/bioinformatics/bts635
38. Liao Y, Smyth GK, Shi W. featureCounts: an efficient general purpose program for assigning sequence reads to genomic features. *Bioinformatics*. 2014;30:923-930. doi:10.1093/bioinformatics/btt656
39. Love MI, Huber W, Anders S. Moderated estimation of fold change and dispersion for RNA-seq data with DESeq2. *Genome Biol*. 2014;15:550. doi:10.1186/s13059-014-0550-8
40. Kolde R, Kolde MR. Package "pheatmap". In: *R Package 1*, 2015:790.
41. Wickham H, Chang W, Wickham MH. Package "ggplot2". In: *Create Elegant Data Visualisations Using the Grammar of Graphics, Version 2*, 2016:1-189.
42. Yu G, Wang L-G, Han Y, He Q-Y. clusterProfiler: an R package for comparing biological themes among gene clusters. *Omics*. 2012;16:284-287.